JCTC Journal of Chemical Theory and Computation

Article

pubs.acs.org/JCTC

Coarse-Grained Potential Model for Structural Prediction of Confined Water

S. Y. Mashayak and N. R. Aluru*

Department of Mechanical Science and Engineering, Beckman Institute for Advanced Science and Technology, University of Illinois at Urbana−Champaign, Urbana, Illinois, 61801 United States

ABSTRACT: We propose a coarse-grained potential model to predict the concentration and potential profiles of confined water. In this model, we represent one water molecule with one coarse-grained bead, such that the interactions between the coarse-grained beads are given by isotropic two-body potentials. Due to the inherent inhomogeneity of the confined water microstructure, we find that a single spatially uniform coarse-grained water−water potential may not be sufficient to accurately predict the structure of water near the surface. To accurately capture surface effects on the water structure, we add a coarse-grained correction potential between wall atoms and water coarse-grained beads. We use an empirical potential-based quasi-continuum theory (EQT) (*J. Chem. Phys.* **2007**, *127*, 174701) to derive and evaluate optimal parameters for the coarse-grained potential model. We evaluate the ability of our model to predict the structure of confined water for two different types of surfaces—a silicon slit channel and a graphite slit channel—and show that the results predicted by EQT are in good agreement with all-atom molecular dynamics results across multiple length scales. We also demonstrate that the coarse-grained potential parameters optimized using EQT work well even in the coarse-grained molecular dynamics simulations.

I. INTRODUCTION

Studying the properties of water confined in different geometries, especially at length scales ranging from a few Angstroms to several nanometers, is important to understand the function of biomolecular systems and enable design of novel nanofluidic and other applications.[1−3] Classical continuum models fail to account for atomistic details of water that are crucial for nanoscale phenomena.[4] Hence, over the past few decades, molecular dynamics (MD) simulations have been used extensively to understand various aspects of water. Accuracy and computational efficiency of MD simulations depend on the level of atomistic detail included and on the potentials describing intramolecular and intermolecular interactions.[5,6] Depending upon the physics of the problem, e.g., chemical reactions, protein folding, electro-osmosis, shocks in fluids, etc., important length and time scales can vary from quantum to atomic to continuum scales.[7] Despite the advancements in computer architecture and in the development of fast algorithms, MD simulations are still very expensive for many applications of practical interest, and accessible time and length scales are limited.

One of the approaches for speeding up the simulation is to reduce the number of degrees of freedom, such as the number of atoms, bonds, bond angles, etc., by systematic coarse graining (CG). In coarse-grained approaches, several atoms are grouped into a single CG site and effective interaction potentials between CG sites are derived from reference all-atom (AA) system, such that the new CG system can mimic the reference system as closely as possible. Several coarse-graining techniques have been developed, such as inverse Boltzmann, inverse Monte Carlo, force matching, and relative entropy, to reproduce various structural and thermodynamic properties of reference AA system.[8−10] CG models, however, suffer from representability and transferability issues, i.e., they cannot simultaneously reproduce all the properties of the reference system and may not be applicable for thermodynamic states other than the reference state.[11,12] Nevertheless, CG models are of great importance for their simplicity, computational efficiency, and suitability for theoretical treatment. Furthermore, with recent advancements, issues of representability and transferability can be addressed.[10,12,13]

In the case of water, anomalous properties, such as the temperature of maximum density (TMD) and the diffusivity increase upon compression (DIC), which are attributed to water's ability to form directional hydrogen bonds, can pose a formidable challenge for coarse graining. CG potentials have been developed to reproduce structural properties of bulk water, such as the radial distribution function (RDF).[9,10,12] Structural properties of confined water can, however, be different from the bulk properties of water. For example, density, RDF, dipole angle distribution, tetrahedral structure, and other properties of water near the surface are different from bulk water and depend upon surface characteristics.[1,3,14] Hence, CG potentials for bulk water cannot capture the structure of confined water accurately. However, not much attention has been given to the development of CG potentials for confined water.

In this paper, we focus on the development of a single-site isotropic two-body coarse-grained potential for confined water at the standard thermodynamic state. We first study characteristics, such as shape, length scales, etc., of a single-site isotropic water−water coarse-grained potential using two of the existing coarse-graining techniques, namely, iterative Boltzmann inversion (IBI)[12] and force matching (FM).[9] We then investigate the limitations of a single spatially uniform coarse-grained potential for confined water due to the surface effects on the water structure. To address the limitations caused by confinement, we

Received: November 22, 2011
Published: March 12, 2012

introduce a coarse-grained correction potential between wall atoms and water coarse-grained beads. We choose the 12−6 Lennard−Jones plus 2 Gaussians functional form to model water−water CG potential and the inverse power plus 2 Gaussians functional form for the wall−water CG correction potential. We use an empirical potential-based quasi-continuum theory (EQT)[15] to optimize these CG potentials for two different kinds of confined water systems—a silicon slit channel and a graphite slit channel—with respect to reference AA SPC/E water model. We then evaluate the ability of the optimized CG potential model to predict the concentration and potential profiles of confined water using EQT and coarse-grained MD simulations.

II. EMPIRICAL POTENTIAL-BASED QUASI-CONTINUUM THEORY (EQT)

EQT[15−17] is a multiscale theory that seamlessly integrates interatomic potentials describing various atomic interactions into the classical continuum theory to predict the structure of confined fluids. It is a simple and fast approach and has been shown to accurately predict the structure of simple Lennard−Jones fluids. In addition to the concentration of confined fluid, the potential profiles describing wall−fluid and fluid−fluid interactions are automatically computed in this approach.

In EQT, for a fluid confined in a slit-like channel, which has two solid walls that are infinite in the x and y directions (see Figure 1), the equilibrium concentration profile, $c(z)$, is

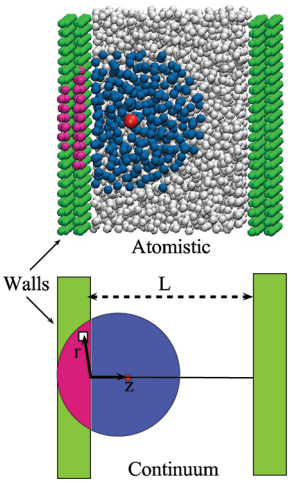

Figure 1. Atomistic (top) and continuum (bottom) representation of confined fluid. Selected fluid atoms (blue) and wall atoms (red) contribute to the total PMF at location z.

determined by solving the 1-D steady-state Nernst−Planck equation

$$\frac{d}{dz}\left(\frac{dc}{dz} + \frac{c}{RT}\frac{dU}{dz}\right) = 0 \tag{1}$$

with boundary conditions

$$c(0) = 0 \tag{2a}$$

$$c(L) = 0 \tag{2b}$$

$$\frac{1}{L}\int_0^L c(z)\mathrm{d}z = c_{\mathrm{avg}} \tag{2c}$$

where U is the total potential of mean force (PMF), T is the fluid temperature, R is the ideal gas constant, L is the channel width, and c_{avg} is the average concentration of the confined fluid, which depends on the thermodynamic state of the fluid and channel width.

To accurately predict the concentration of the confined fluid from eq 1, the total PMF, U, needs to be computed correctly. For a confined fluid system, the total PMF is due to wall−fluid and fluid−fluid interactions and can be computed as the sum of the wall−fluid PMF, U^{wf}, and the fluid−fluid PMF, U^{ff}, i.e.

$$U(z) = U^{\mathrm{wf}}(z) + U^{\mathrm{ff}}(z) \tag{3}$$

In EQT, a continuum approximation is used to compute the wall−fluid PMF and the fluid−fluid PMF. In a continuum approximation, the wall atoms are represented by a density, c_{wall}, and for a given wall−fluid pair interaction, u^{wf}, the wall−fluid PMF, U^{wf}, is computed as

$$U^{\mathrm{wf}}(z) = \int_V u^{\mathrm{wf}}(|z - r|)c_{\mathrm{wall}}(r)\mathrm{d}V \tag{4}$$

where r is the location of infinitesimal volume, $\mathrm{d}V$, of wall atoms and V is the total volume of wall atoms contributing to the wall−fluid PMF at location z (see Figure 1). Similarly, the fluid atoms are represented by a concentration, c, and for a given fluid−fluid pair interaction, u^{ff}, the fluid−fluid PMF, U^{ff}, is computed as

$$U^{\mathrm{ff}}(z) = \int_V u^{\mathrm{ff}}(|z - r|)c(r)\mathrm{d}V \tag{5}$$

Determination of U^{ff} by eq 5 requires core-softened u^{ff}. Usually, fluid−fluid pair potentials have hard cores, i.e., $u(r) \to \infty$ as $r \to 0$. Hence, in a continuum approximation, to avoid singularity, the hard core part of u^{ff} must be replaced by a structurally consistent soft core, i.e., u^{ff} should be finite as $r \to 0$. References 15 and 16 discuss formulations of core-softened u^{ff} for simple Lennard−Jones fluids, and single-site core-softened potentials for the graphite−CO_2 system are discussed in ref 17. Also, in eq 5, we use the mean field approximation (MFA), where correlations between concentration are neglected. Similar MFA has been used in devising approximate density functionals for excess Helmholtz energy in classical density functional theory (cDFT).[18−20] We note that EQT fluid−fluid potential formulation based on MFA and soft-core pair potential can also be used to formulate an approximate functional for excess Helmholtz energy in cDFT. Then, following the standard cDFT approach of the functional minimization,[21] we get

$$RT \ln c + U = \mathrm{const} \tag{6}$$

Equation 6 expresses that the chemical potential of the confined fluid should be equal everywhere at equilibrium.[22] The Nernst−Planck equation, eq 1, also ensures the uniform chemical potential inside the confinement, since it is mathematically equivalent to eq 6.

In the case of water, determination of potentials using atomistic water models, such as SPC/E, TIP3P, TIP5P, etc., requires detailed information about coordinates of oxygen and hydrogen atoms of water molecules. In a continuum approximation, where water molecules are represented by their concentration, PMF computations by eqs 3, 4, and 5 using atomistic potential models may not be possible if we do not know the relative positioning of the internal degrees of water molecules a priori. Hence, we develop a coarse-grained

Table 1. Average Concentration in Various Size Channels

system	20σ	11σ	10σ	9σ	8σ	7σ	6σ	5σ	4σ	3σ	2σ
silicon−water	33.00	33.18	32.87	32.49	32.03	31.45	30.69	29.75	28.59	24.32	18.0
graphite−water	33.00	33.26	32.87	32.40	31.79	31.03	30.09	28.89	25.25	22.64	19.0

potential model for confined water in which atomistic degrees of freedom of the water molecule are coarse grained into a single site located at the center of mass (COM) and effective single-site isotropic potentials for water−water and wall−water interactions are derived.

III. MD SIMULATION DETAILS

We simulated water structure in two types of slit−channel systems, namely, the silicon−water system and graphite−water system. The silicon−water system considered here is similar to the one used in ref 4. It consists of water molecules confined between two slabs of silicon (Si) walls. Each Si wall consists of four layers of Si atoms oriented in the ⟨111⟩ direction, and the separation distance between the first and the second layer is 0.078 nm, the second and the third layer is 0.236 nm, and the third and the fourth layer is 0.078 nm. Each layer of the wall is made of 161 Si atoms, and the lateral dimensions of the wall are 4.66 × 4.43 nm^2. In the graphite−water system, water molecules are confined between two slabs of graphite walls. Each graphite wall consists of four graphene layers, with an interlayer spacing of 0.335 nm, and the lateral dimensions of the wall are 4.550 × 4.331 nm^2. In both systems, the channel width is varied between 2σ and 20σ, where σ (= 0.317 nm) is the length parameter for the Lennard−Jones interaction between oxygen atoms of water molecules. The thermodynamic state of the confined water in all channel widths corresponds to that of the bulk water at the standard thermodynamic state, i.e., 300 K temperature and 1.0 g/cm^3 (c_{bulk} = 33.0 atoms/nm^3) density.

In MD simulations, the total number of molecules, N, of the confined fluid, which is in equilibrium with the bulk fluid at a given density and temperature, must be specified a priori. N can be obtained if we know the average concentration of the confined fluid defined as $c_{avg} = N/V_{channel}$, where $V_{channel}$ is the volume of the channel. It is, therefore, required to determine c_{avg} of confined water for various separations of the channel walls. In this work, to determine the average concentration of confined water in equilibrium with the bulk water at the standard thermodynamic state, we adopt the linear superposition approximation (LSA), as described in ref 23. It was shown in ref 23 that c_{avg} of confined water at various separations obtained using LSA is thermodynamically consistent except at very small separations. Hence, we use LSA to determine c_{avg} for channels of widths larger than 4σ, and for smaller channels, we performed equilibration simulations with the channel attached to the bulk water reservoir at 1 bar pressure and 300 K temperature and counted the total number of water molecules inside the channel at equilibrium. The c_{avg} values obtained using this procedure are given in Table 1.

All-atom molecular dynamics (AA-MD) simulations are performed in the NVT (canonical) ensemble using GROMACS 4.0.7.[24] Water is modeled using the extended simple point charge (SPC/E)[25] model; the interaction parameters used in these simulations are given in Table 2. The Lennard−Jones interactions are computed using a spherical cutoff of 1.5 nm, and water−water electrostatic interactions are computed using the particle mesh Ewald (PME)[26] method with an extra vacuum above the surface along with an appropriate correction for the slab geometry. Wall atoms are fixed at their original positions. Periodic boundary conditions are specified in the x and y directions. Temperature is maintained at 300 K using the Nosé−Hoover thermostat[27] with a 0.1 ps time constant. The system is integrated using a time step of 1 fs.

Table 2. Interaction Parameters Used in All-Atom MD Simulations

	σ (nm)	ε (kJ/mol)	q (e)
O	0.317	0.6503	−0.8476
H	0.0	0.0	0.4238
Si	0.3385	2.4522	0.0
C	0.3390	0.2334	0.0
Si−O	0.3275	1.2628	
C−O	0.3280	0.3896	

We also performed coarse-grained MD (CG-MD) simulations using the CG potential model for confined water developed in this work. CG-MD simulations were performed using GROMACS 4.0.7 with the same system settings as for the all-atom simulations, except that the CG interactions are specified using tabulated potentials.

IV. DEVELOPMENT OF CG MODEL

A. Functional Form. In the CG model for the confined water system, we represent one water molecule with one coarse-grained bead at the center of mass (COM) and retain all the atomistic details of the channel wall. This representation is similar to the hybrid simulations approach used in ref 28 in which part of the system is represented at atomic resolution and the remaining part at coarse-grained level. In this hybrid representation of the confined water system, we need to specify the effective interaction potentials between water−water CG beads and between wall−water CG beads. In the reference all-atom models, silicon wall atoms and graphite wall atoms are modeled as simple LJ-type atoms, and hence, the interaction between the wall atom and the water molecule is already a single-site potential. Therefore, in our CG model, we use the same reference all-atom model's 12-6 LJ potential for the interaction between the wall atom and the water CG bead. The objective, therefore, is to determine the water−water coarse-grained potential.

In general, coarse-grained potentials cannot simultaneously reproduce all the properties of the reference all-atom system.[11,12,29] In this work, the goal of the CG model is to reproduce, as accurately as possible, the equilibrium COM concentration profile of confined water predicted by reference AA-MD simulations. We note that for the SPC/E water model differences between the COM concentration profile and the water oxygen concentration profile are almost negligible.

Due to the inherent inhomogeneity of the confined water system and water's special characteristic of forming directional hydrogen bonds, it is a formidable problem to parametrize a single-site isotropic CG potential model for confined water. To our knowledge, there is no systematic method for parametrizing CG potentials to reproduce the concentration profile of

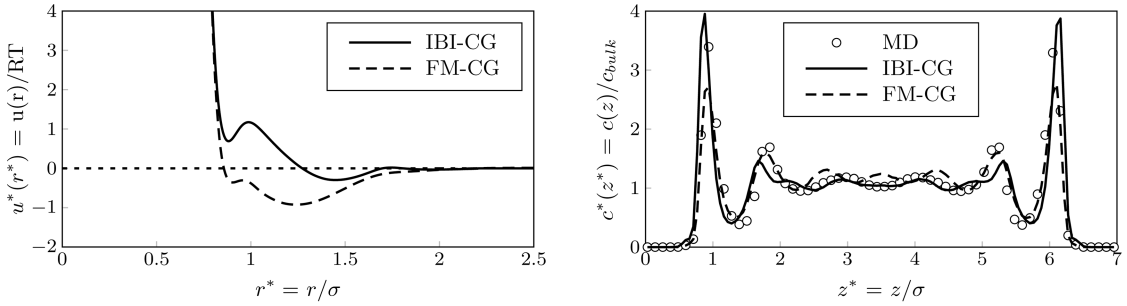

(a) Water-water coarse-grained potentials.

(b) Comparison of AA-MD and CG-MD water COM concentration profiles in the 7σ silicon-water channel.

Figure 2. Evaluation of coarse-grained potentials obtained by iterative Boltzmann inversion (IBI) and force-matching (FM) coarse-graining techniques.

confined fluids. We, however, first investigate two of the various coarse-graining techniques available in the literature,[8−10,12,30,31] namely, iterative Boltzmann inversion (IBI)[12] and force matching (FM).[9] We use open-source VOTCA code, developed by Rühle et al.,[8] to determine these two potentials.

The IBI method optimizes the CG potential to reproduce the target RDF of CG beads. Due to the inhomogeneity of the water channel system, the local microstructure of the water molecule, such as RDF, is not uniform in the transverse direction.[14] Hence, instead of the confined water RDF, we use the bulk water COM RDF as the target for IBI and obtain the coarse-grained potential IBI-CG, which is shown in Figure 2a. We then test this potential by performing CG-MD simulations on the 7σ silicon−water channel system. From the CG-MD results, shown in Figure 2b, we observe that the IBI-CG potential fails to predict the interfacial layering of water accurately. This is not unusual because the structure of interfacial water is quite different from that of bulk water.[14] Eslami et al.[32] also noted that the potentials derived from RDF may not reproduce the surface-induced density profiles of confined fluids accurately.

The FM method optimizes the CG potential to match, as closely as possible, forces on the CG sites from the reference all-atom simulations. The FM technique has been used, first by Izvekov and Voth[9] and later by Rühle et al.,[8] to develop CG potentials for bulk water. They have shown that the CG potential obtained by FM qualitatively reproduces the structure of bulk water. Here, we use the 7σ silicon−water channel as the reference system for the FM technique and obtain the coarse-grained potential FM-CG, which is shown in Figure 2a. We then use this potential in CG-MD simulations of the same 7σ silicon−water channel. From the CG-MD results, shown in Figure 2b, we observe that the FM-CG potential captures the interfacial region better compared to the central bulk-like region, where it introduces excessive oscillations in the concentration profile compared to the AA-MD results.

Although IBI-CG and FM-CG potentials do not accurately predict the confined water structure, they provide significant insights into the characteristics of the CG potential for confined water. When we compare IBI-CG and FM-CG potentials, we observe that they both are core-softened double-well-type potentials, similar to the single-site water potentials studied earlier.[10,33−35] They, however, differ in the depth of both wells and the location of the second well. The location of the first well is almost the same, i.e., around 0.28 nm, which is representative of the water's first coordination shell. We also note that the difference between the magnitude of the first peak and the magnitude of the second well of the IBI-CG potential is greater than that of the FM-CG potential. Wang et al.[12] suggest that the difference between the magnitude of the first peak and the magnitude of the second well of the water CG potential governs the tetrahedral packing of water molecules: the larger the difference, the stronger is the tetrahedral packing. This implies that the FM-CG potential introduces a weaker tetrahedral packing compared to the IBI-CG potential. It is known that for water confined between uncharged walls tetrahedral packing of water molecules is not uniform and is weaker near the interface compared to the bulk-like region.[14,36] Hence, weaker tetrahedral packing may be one of the reasons for stronger oscillations of concentration in the bulk-like region predicted by the FM-CG potential. Further, CG-MD results using IBI-CG and FM-CG potentials suggest that, due to the inhomogeneity in the confined water microstructure, a single spatially uniform water−water CG potential may not be sufficient to accurately capture the water structure in all regions of the channel.

With this understanding, we now focus our attention on the development of a more accurate CG potential model for the confined water system. First, we define the functional forms to model various interactions in the CG system. As mentioned above, for the wall−fluid CG pair interaction, we use the same 12-6 LJ potential as employed in the reference all-atom MD simulations, i.e.

$$u_{LJ}^{wf}(r) = 4\varepsilon_{wf}\left(\frac{\sigma_{wf}^{12}}{r^{12}} - \frac{\sigma_{wf}^{6}}{r^{6}}\right) \tag{7}$$

where ε_{wf} and σ_{wf} are the usual LJ parameters (see Table 2). For the fluid−fluid CG pair interaction, to capture the double-well core-softened potential, we use the 12-6 Lennard−Jones plus 2 Gaussians (LJ2G) functional form given by

$$u_{LJ2G}^{ff}(r) = 4\varepsilon_{ff}\left(\frac{\sigma_{ff}^{12}}{r^{12}} - \frac{\sigma_{ff}^{6}}{r^{6}}\right) + \lambda_{1,ff}\exp\left(-\left(\frac{r-\mu_{1,ff}}{h_{1,ff}}\right)^2\right) + \lambda_{2,ff}\exp\left(-\left(\frac{r-\mu_{2,ff}}{h_{2,ff}}\right)^2\right) \tag{8}$$

where λ, μ, and h are the Gaussian parameters determining the magnitude, center, and width, respectively. Superposition of LJ and one Gaussian (LJG) has been previously used to

model bulk water CG potentials by Chaimovich and Shell[10] and Cho et al.[34]

As explained before, a single spatially uniform water−water CG potential may not be able to reproduce the structure of confined water near the interface and in the bulk-like region simultaneously. Hence, to account for the inhomogeneity of the confined water microstructure, we introduce a coarse-grained correction (CGC) potential. The objective of the CGC potential is to correct the structure of water near the surface. Hence, the CGC potential should act only on the water CG beads which are near the surface. One approach to achieve this is to employ the correction potential through wall−fluid interactions. We, therefore, model CGC potential as an additional pair interaction, along with the original 12-6 LJ potential, between the wall atom and the water CG site. The need for such a systematic correction to reproduce the water structure around the methane solute is also mentioned in ref 37, where the methane−water interaction length parameter was increased by ∼0.025 nm to accurately capture the solute−water PMF. In this work, for generality, we use the inverse power plus 2 Gaussians functional form for the CGC potential, i.e.

$$u^{\mathrm{wf}}_{\mathrm{CGC}}(r) = 4\varepsilon_{\mathrm{CGC}}\left(\frac{\sigma^{m}_{\mathrm{CGC}}}{r^{m}} - \frac{\sigma^{n}_{\mathrm{CGC}}}{r^{n}}\right) + \lambda_{1,\mathrm{CGC}}\exp\left(-\left(\frac{r-\mu_{1,\mathrm{CGC}}}{h_{1,\mathrm{CGC}}}\right)^{2}\right) + \lambda_{2,\mathrm{CGC}}\exp\left(-\left(\frac{r-\mu_{2,\mathrm{CGC}}}{h_{2,\mathrm{CGC}}}\right)^{2}\right) \tag{9}$$

where m and n are the usual power terms in the inverse power form and the other parameters have the same definitions as in eq 8. Note that the superscript wf is used for the correction potential, $u^{\mathrm{wf}}_{\mathrm{CGC}}$, to denote that it is an interaction between the wall atom and the water CG bead.

Next, we need to optimize the CG potential parameters in eqs 8 and 9 with respect to the reference AA confined water system. To optimize and evaluate the CG potential parameters we choose EQT, which is a computationally more efficient method compared to CG-MD simulations. Before we can employ the proposed CG potentials in EQT, we need to make sure that they do not introduce any numerical singularity in a continuum approximation and if necessary, as explained before, an appropriate soft-core form should be used. The details of the soft-core coarse-grained potential for EQT and the CG potential optimization procedure are given in the following subsection.

B. Soft-Core Coarse-Grained Potential. In the EQT framework, first, we need to derive the PMF formulations using the proposed CG potentials, given by eqs 7, 8, and 9. The wall−fluid PMF, $U^{\mathrm{wf}}_{\mathrm{LJ}}$, can be computed in the usual way by substituting the wall−fluid pair potential, $u^{\mathrm{wf}}_{\mathrm{LJ}}$ (eq 7), in the wall−fluid PMF formulation given by eq 4. The detailed description of the wall−fluid PMF formulation is given in the Appendix. We can observe from eq 8 that $u^{\mathrm{ff}}_{\mathrm{LJ2G}}(r) \to \infty$ as $r \to 0$. Hence, in EQT, to avoid numerical singularity while computing the fluid−fluid PMF, U^{ff}, using eq 5, we replace the hard-core part of the $u^{\mathrm{ff}}_{\mathrm{LJ2G}}$ with the soft core. We use a quadratic polynomial to model the soft core, and the soft-core form of the water−water CG potential, $u^{\mathrm{ff}}_{\mathrm{LJ2G-Soft}}$, employed in EQT, is given by

$$u^{\mathrm{ff}}_{\mathrm{LJ2G-Soft}}(r) = \begin{cases} 0, & r \le R_{\mathrm{crit}} \\ a_0 + a_1(r - R_{\mathrm{min}}) + a_2(r - R_{\mathrm{min}})^2, & R_{\mathrm{crit}} < r \le R_{\mathrm{min}} \\ u^{\mathrm{ff}}_{\mathrm{LJ2G}}(r), & r > R_{\mathrm{min}} \end{cases} \tag{10}$$

where R_{crit} and R_{min} define the region of the soft-core part and a_0, a_1, and a_2 are algebraic coefficients. a_0 is determined such that C^0 continuity is satisfied at R_{min}, i.e., $u^{\mathrm{ff}}_{\mathrm{LJ2G-Soft}}(R_{\mathrm{min}}) = u^{\mathrm{ff}}_{\mathrm{LJ2G}}(R_{\mathrm{min}})$, and a_1, a_2, R_{crit}, and R_{min} need to be optimized along with the LJ2G parameters. Although, the correction potential is employed as a wall−fluid interaction, it is effectively a fluid−fluid interaction phenomena; hence, we consider it in the fluid−fluid PMF computations. We compute the total fluid−fluid PMF, U^{ff}, in three steps. First, we compute the LJ2G fluid−fluid PMF, $U^{\mathrm{ff}}_{\mathrm{LJ2G}}$, by substituting the soft-core form of the LJ2G fluid−fluid pair potential, $u^{\mathrm{ff}}_{\mathrm{LJ2G-Soft}}$ (eq 10), in the fluid−fluid PMF formulation given by eq 5. Then, we compute the correction PMF, $U^{\mathrm{wf}}_{\mathrm{CGC}}$, by substituting the CGC pair potential, $u^{\mathrm{wf}}_{\mathrm{CGC}}$ (eq 9), in the wall−fluid PMF formulation given by eq 4. Finally, we compute the total fluid−fluid PMF, U^{ff}, as a sum of the LJ2G fluid−fluid PMF, $U^{\mathrm{ff}}_{\mathrm{LJ2G}}$, and the correction PMF, $U^{\mathrm{wf}}_{\mathrm{CGC}}$, i.e.,

$$U^{\mathrm{ff}}(z) = U^{\mathrm{ff}}_{\mathrm{LJ2G}}(z) + U^{\mathrm{wf}}_{\mathrm{CGC}}(z) \tag{11}$$

The detailed description of $U^{\mathrm{ff}}_{\mathrm{LJ2G}}$ and $U^{\mathrm{wf}}_{\mathrm{CGC}}$ formulations is given in the Appendix. The total PMF, U, is then computed as

$$U(z) = U^{\mathrm{wf}}_{\mathrm{LJ}}(z) + U^{\mathrm{ff}}(z) \tag{12}$$

The objective of the CG model is to reproduce the COM concentration profile of confined water predicted by AA-MD simulations. In the canonical ensemble reference atomistic simulations, the equilibrium concentration profile, $c(z)$, is related to the total PMF, $U(z)$, through the Boltzmann distribution law given as

$$c(z) = c_0 \exp\left(-\frac{U(z)}{kT}\right) \tag{13}$$

where k is the Boltzmann constant and c_0 is the concentration at the reference point used for the PMF computations; here, we use the midpoint of the channel as the reference point. This implies that reproducing the total PMF profile, $U(z)$, is equivalent to reproducing the concentration profile of the confined fluid. Therefore, the objective function for the CG model parameter optimization can be defined as

$$\underset{X}{\text{minimize}} \left| U(X, c^{\mathrm{target}}, z) + kT \ln\left(\frac{c^{\mathrm{target}}(z)}{c_0}\right)\right| \tag{14}$$

Table 3. Silicon−Water System: Coarse-Grained Model Potential Parameters[a]

potential	m	n	σ	ε	λ_1	μ_1	h_1	λ_2	μ_2	h_2
u_{LJ}^{wf}	12.0	6.0	0.3275	1.2628						
u_{LJ2G}^{ff}	12.0	6.0	0.25	21.2	26.4304	0.247	0.11	0.3	0.54	0.1
u_{CGC}^{wf}	7.0	6.0	0.266	12.0	20.0	0.17	0.15			
	R_{crit}	R_{min}	a_0	a_1	a_2					
soft core	0.0	0.2637	8.9314	−200.0	−250.0					

[a]Length parameters in nm; energy parameters in kJ/mol.

Table 4. Graphite−Water System: Coarse-Grained Model Potential Parameters[a]

potential	m	n	σ	ε	λ_1	μ_1	h_1	λ_2	μ_2	h_2
u_{LJ}^{wf}	12.0	6.0	0.3280	0.3896						
u_{LJ2G}^{ff}	12.0	6.0	0.25	21.2	26.4304	0.247	0.11	0.3	0.54	0.1
u_{CGC}^{wf}	7.0	6.0	0.26	3.0	20.0	0.10	0.15			
	R_{crit}	R_{min}	a_0	a_1	a_2					
soft core	0.0	0.2637	8.9314	−200.0	−250.0					

[a]Length parameters in nm; energy parameters in kJ/mol.

where X denotes the CG parameters that are to be determined, i.e.

$$X = [R_{crit}, R_{min}, a_1, a_2, \varepsilon_{ff}, \sigma_{ff}, \lambda_{1,ff}, \mu_{1,ff}, h_{1,ff}, \lambda_{2,ff}, \mu_{2,ff}, h_{2,ff}, m, n, \varepsilon_{CGC}, \sigma_{CGC}, \lambda_{1,CGC}, \mu_{1,CGC}, h_{1,CGC}, \lambda_{2,CGC}, \mu_{2,CGC}, h_{2,CGC}]$$

and $U(X,c^{target},z)$ is the total PMF computed by EQT using the target concentration profile, $c^{target}(z)$.

Another alternative approach to determine the water−water CG potential and the wall−water correction potential is to use the force matching with *exclusions* method described by Rühle and Junghans in ref 38. In this method, first the water−water CG potential can be optimized such that the forces due to only water−water interactions on the water CG beads in the bulk-like region are reproduced. Then, the wall−water correction potential can be optimized such that the correction forces, i.e., total reference force − (wall−water 12−6 LJ force + water−water CG potential force), acting on the water CG beads near the surface are reproduced. However, we use the objective function defined in eq 14, which is equivalent to a potential matching scheme, to optimize the CG parameters as it directly relates the CG parameters to the target density profile.

It is known that the structural properties of confined water depend on the type of the channel wall and the width of the channel.[14] As mentioned above, the CG model parameters are optimized using the concentration and the PMF profiles from the reference all-atom MD simulations. Here, we optimize the CG model parameters independently for the silicon−water system and for the graphite−water system using the 7σ channel concentration profile of the respective system as the target concentration, $c^{target}(z)$. We find that, as described in the Results section, the CG potential parameters optimized for one channel width of the confined water system are transferrable across all the channel widths of the same system at the same thermodynamic state. In addition, the parameters optimized for EQT are found to work reasonably well even in the CG-MD simulations.

The problem of optimizing the CG model parameters is highly nonlinear, and substantial coupling between the potential parameters makes it even more challenging. Some knowledge about the physical significance of the various CG parameters can help in determining the parameters efficiently. We ensure that $0 \le R_{crit} < R_{min} < 0.28$ nm, so that the soft core is only enforced where the LJ2G potential is strongly repulsive, and all the essential features of the double-well core-softened water CG potential are preserved. Since the IBI-CG potential seems to work well in the bulk-like region, we also ensure that the LJ2G potential does not deviate much from the IBI-CG potential. Also, we make sure that the CGC potential is short range, so that it is effective only near the channel wall.

The optimized CG potential parameters for the silicon−water system and the graphite−water system are given in Tables 3 and 4, respectively. Note that for both systems the wall−fluid potential (u_{LJ}^{wf}) parameters are the same as those used in AA-MD simulations. We find that the same LJ2G potential and the soft-core parameters are applicable in the silicon−water and the graphite−water systems. This can be understood by noting that the LJ2G potential is optimized to capture the water structure in the bulk-like region, and in both systems, the water microstructure away from the wall, i.e., in the bulk-like region, is very similar. However, the optimum CGC potential parameters, which are optimized to capture the interfacial water layer, are different for the two systems. This can be attributed to the different interfacial microstructure of water near the silicon wall and the graphite wall due to the differences in the wall structure and the wall−fluid interaction parameters. We find that the second Gaussian term in the CGC potential functional form, eq 9, is unnecessary in the case of the silicon−water and the graphite−water systems, but it may be useful in a different wall channel system.

Figure 3 shows the optimized LJ2G potential along with the soft core. It can be observed that the LJ2G potential does retain the core-softened double-well shape and does not deviate much from the IBI-CG potential. Also, we note that the location of the first well is at 0.3 nm, which is very close to the water's first coordination shell location. Remarkably, the ratio of the location of the first well to the location of the second well is 0.68, which is in agreement with the observation made by Stanley et al.,[13] that in order to have water-like characteristics this ratio should be ∼0.6.

Figure 4a and 4b shows the CGC potentials along with the wall−fluid LJ potentials for the silicon−water and graphite−water

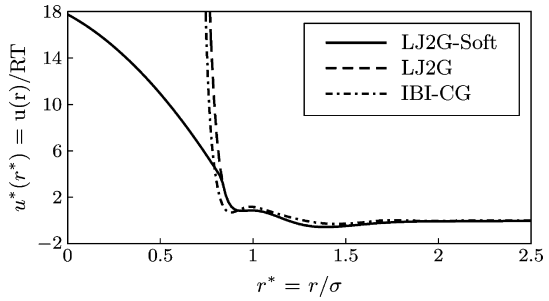

Figure 3. Water−water coarse-grained potentials optimized for confined water (LJ2G and LJ2G with soft core) and bulk water (IBI-CG).

systems, respectively. It can be observed that in both systems the correction potential has a softer repulsive core compared to the wall−fluid LJ potential, and it has an attractive energy part before it smoothly goes to 0. This suggests that the LJ2G potential, which is optimized for the bulk-like region, is not attractive enough to capture the interfacial water layers; hence, the correction potential is required to account for the missing attractive energy near the channel walls.

V. RESULTS

A. EQT Simulations. Just as in MD simulations, the input parameters needed to perform EQT simulations are the interaction potential parameters, the wall structure (the dimensions of the wall and the wall atom density c_{wall}), the channel width L, and the average concentration c_{avg} of water inside the channel (see Table 1). Once the input parameters are specified, an iterative scheme can be used to solve eqs 1, 11, 12, A7, A11, and A13 in a self-consistent manner to compute the concentration and potential profiles of confined water. The numerical algorithm to perform EQT simulations is discussed in ref 15.

1. Silicon−Water System. In EQT computations, each wall of the silicon channel, as described in section III, is represented by two continuum layers of thickness 0.078 nm and separated by a distance of 0.236 nm. Each layer has a silicon atom concentration of 200 atoms/nm^3, i.e., c_{wall} = 200. First, we perform EQT simulations on the 7σ channel for which the CG model parameters are optimized. The results, shown in Figure 5, indicate that the COM concentration and various PMF profiles of water predicted by EQT match well with AA-MD simulations. EQT, however, overpredicts the magnitude of the first interfacial layer (see Figure 5a). As discussed in ref 15, this behavior is attributed mainly to the slight overprediction of the wall−fluid PMF around 1σ distance away from the surface due to the continuum approximation of wall−fluid interactions. Also, near the surface, the fluid−fluid PMF from EQT is more repulsive compared to the fluid−fluid PMF from AA-MD. The discrepancy in the fluid−fluid PMF from EQT is due to the correction PMF. As we try to optimize the CG model parameters so that the target total PMF is reproduced, the correction PMF not only compensates for the limitations of the LJ2G PMF near the surface but also tries to account for the overprediction of the wall−fluid PMF.

Next, we use the same CG parameters and compute the structure of water in different silicon−water channel widths at the same thermodynamic state, and these results are shown in Figure 6. We observe that EQT predictions for COM concentration profiles of water are in good agreement with AA-MD results. This suggests that the CG parameters are transferable across multiple channel widths of the silicon−water system at the same thermodynamic state. We also perform EQT simulation of the water structure in a very large silicon−water channel, i.e., 100σ channel, for which AA-MD simulations are intractable. Figure 7 shows that EQT can efficiently predict the structure of water near the surface of very large channels as well.

2. Graphite−Water System. For EQT simulations on the graphite−water system, each layer of the graphite wall, i.e., each graphene layer (see secton III for details), is approximated as a continuum surface with carbon atom surface concentration of 40.49 atoms/nm^2, i.e., c_{wall} = 40.49. Similar to the silicon−water system, we first test the CG model of the graphite−water system for the reference 7σ channel. From Figure 8, we observe that the COM concentration and various PMF profiles of water from EQT match well with AA-MD results. The discrepancies in the fluid−fluid PMF and the concentration near the surface are due to the same reasons, as explained in the case of silicon−water system. Figure 9 shows that the CG model parameters of the graphite−water system are transferable across multiple channel widths at the same thermodynamic state.

B. CG-MD Simulations. To check the physical consistency of the CG potential model optimized for EQT, we perform CG-MD simulations using the CG potential. In CG-MD, since there is no issue of numerical singularity, we use the hard-core form of the LJ2G (eq 8) instead of the soft-core form. From Figures 10 and 11, we observe that CG-MD predictions of COM concentration profiles of water in silicon−water and graphite−water channels of different widths match reasonably well with AA-MD results, verifying that the CG parameters, used in EQT, are physically consistent.

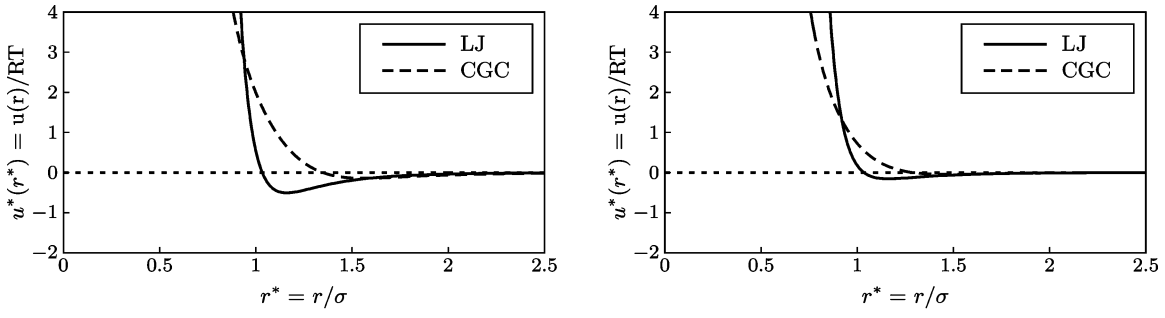

(a) Silicon-water system. (b) Graphite-water system.

Figure 4. Lennard−Jones (LJ) and coarse-grained correction (CGC) wall−fluid potentials for the silicon−water system and graphite−water system.

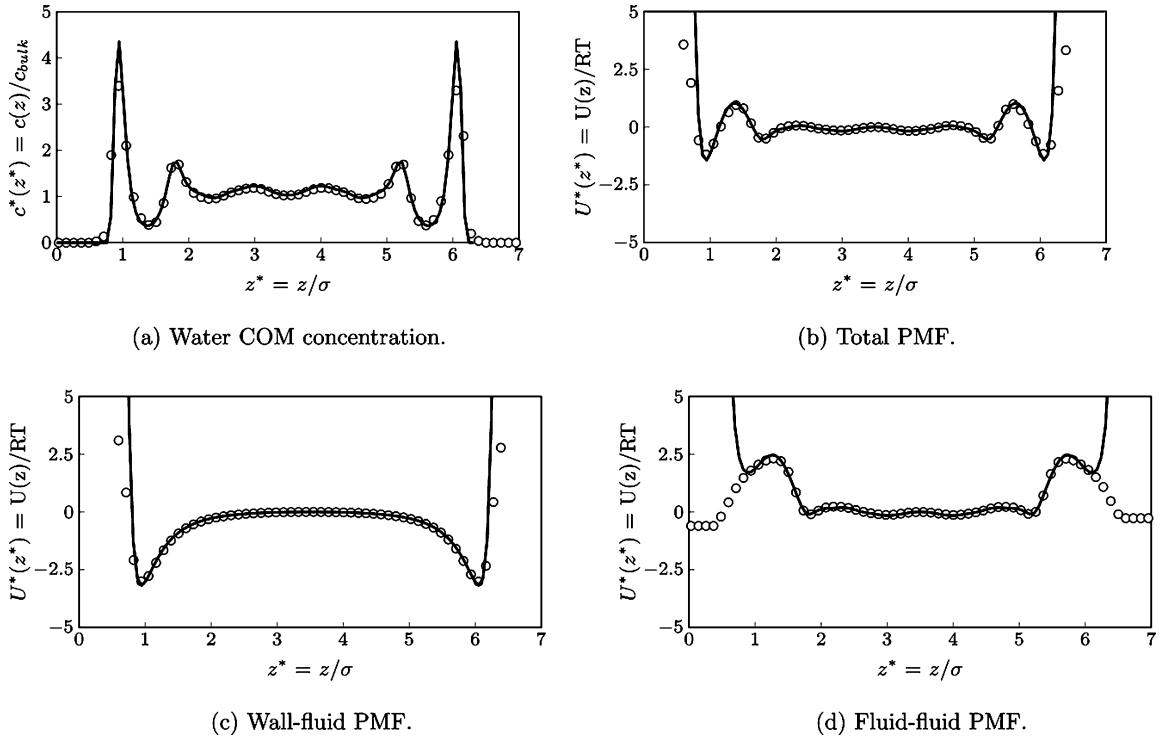

(a) Water COM concentration. (b) Total PMF.

(c) Wall-fluid PMF. (d) Fluid-fluid PMF.

Figure 5. EQT predictions of water COM concentration and potential profiles in the 7σ silicon−water channel. Lines are EQT results, and circles are AA-MD results.

VI. CONCLUSIONS

In this paper, we developed an accurate coarse-grained potential model for structural prediction of confined water. We showed that the coarse-grained potential optimized for bulk water does not capture the surface-induced structure of confined water. We demonstrated that due to the inhomogeneity of the water microstructure in the channel a single spatially uniform water−water coarse-grained potential cannot reproduce the structure of water near the surface and in the bulk-like region simultaneously. To address this issue, we introduced a correction potential which acts only on the interfacial region. We then used these CG potentials in empirical potential-based quasi-continuum theory (EQT) simulations to predict the density profiles of confined water in the silicon and the graphite slit-like channels. EQT results are found to be in good agreement with those obtained from AA-MD simulations. We also showed that EQT is a computationally efficient framework compared to atomistic approaches, and it can be used to predict the structure of confined water at multiple length scales. The physical consistency of the confined water CG model is also checked by performing coarse-grained MD simulations, and the results from CG-MD simulations are found to be in reasonable agreement with AA-MD simulations.

APPENDIX A: EQT POTENTIAL FORMULATIONS FOR WATER

1. Fluid−Fluid Potential

As shown in Figure 12, the fluid−fluid LJ2G potential at location z, $U^{ff}_{LJ2G}(z)$, can be computed as a sum of interactions with all the neighboring CG water beads, i.e.

$$U^{ff}_{LJ2G}(z) = \sum_{i=1}^{N_b} u^{ff}_{LJ2G}(|z - R_i|) \tag{A1}$$

where N_b is the total number of neighbors within the cut-off distance, r_{cut}, from z and R_i is the position of CG bead i. Representing CG beads by their concentration, c, and substituting $r_i = |z-R_i|$, we can rewrite eq A1 as

$$U^{ff}_{LJ2G}(z) = \sum_{i=1}^{N_v} u^{ff}_{LJ2G}(r_i)c(r_i)\Delta V_i \tag{A2}$$

where N_v denotes the total number of discrete volumes ΔV into which the neighboring region is divided. The continuum approximation for the discrete summation in eq A2 is

$$U^{ff}_{LJ2G}(z) = \int_V u^{ff}_{LJ2G}(r)c(r)\mathrm{d}V \tag{A3}$$

Since for the channel system under investigation variation of c is only in the z direction, we divide the neighboring volume V into circular disks with thickness dz' (see Figure 12), and the contribution to the LJ2G fluid−fluid potential at z due to a circular disk at location z', $dU^{ff}_{LJ2G}(z')$, can be computed as

$$dU^{ff}_{LJ2G}(z') = \left(\int_0^{s_{cut}} u^{ff}_{LJ2G}(s)2\pi s\ \mathrm{d}s\right)c(z')dz' \tag{A4}$$

where $s = (r^2 - (z-z')^2)^{1/2}$. Substituting $r = (s^2 + (z-z')^2)^{1/2}$

$$dU^{ff}_{LJ2G}(z') = \left(\int_{|z-z'|}^{r_{cut}} u^{ff}_{LJ2G}(r)2\pi r\ \mathrm{d}r\right)c(z')dz' \tag{A5}$$

As the LJ2G potential smoothly goes to 0, we can substitute $r_{cut} = \infty$ and the total LJ2G fluid−fluid potential can be computed as

$$U^{ff}_{LJ2G}(z) = \int_0^L 2\pi c(z')\left(\int_{|z-z'|}^{\infty} u^{ff}_{LJ2G}(r)r\ \mathrm{d}r\right)\mathrm{d}z' \tag{A6}$$

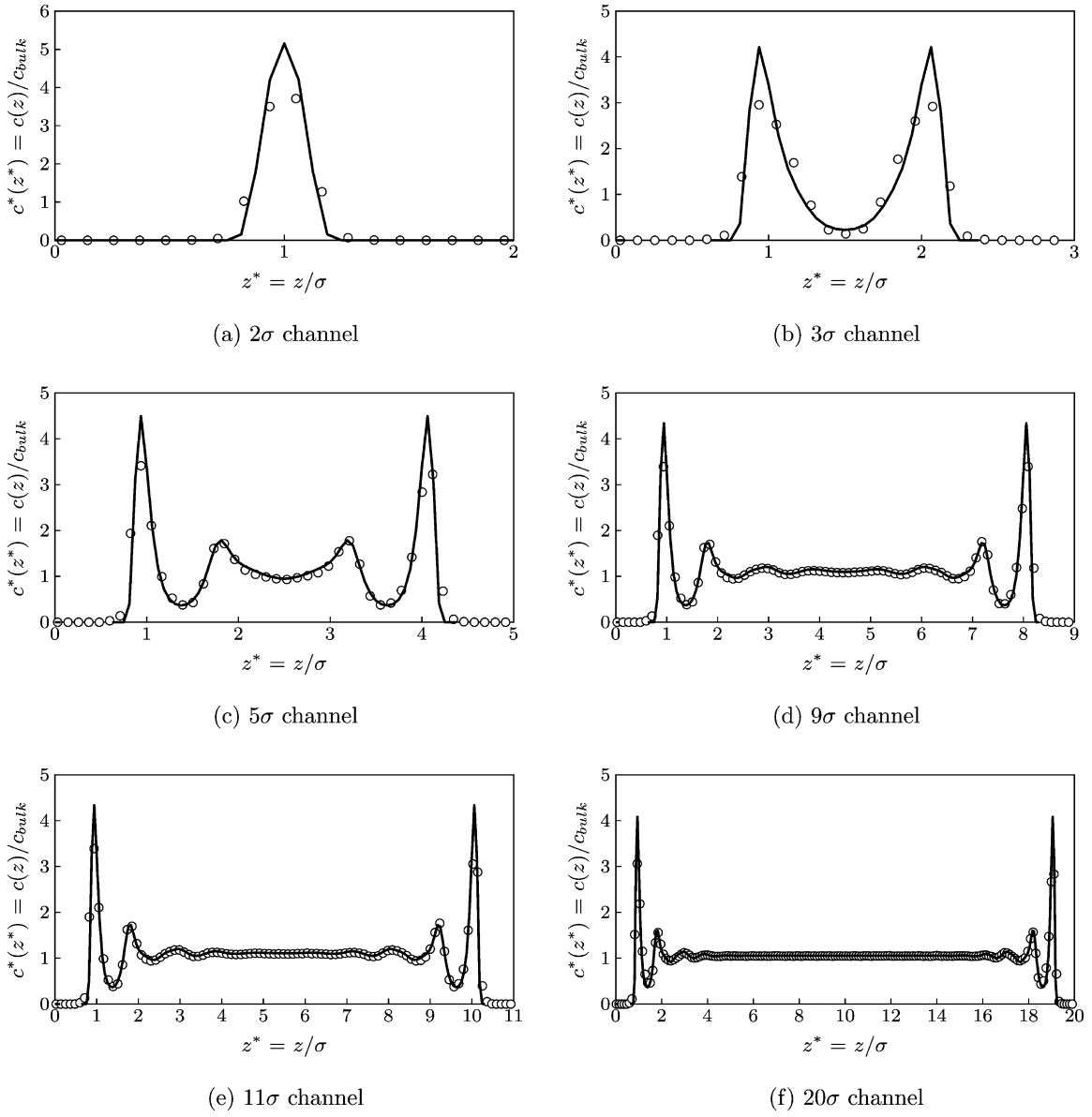

Figure 6. Silicon−water channel: EQT predictions of water COM concentration profiles in different channel widths. Lines are EQT results, and circles are AA-MD results.

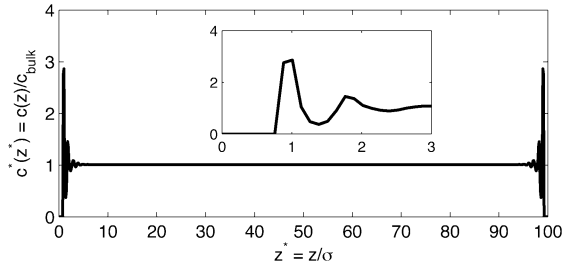

Figure 7. EQT prediction of water COM concentration profile in the 100σ silicon−water channel.

As explained in the paper, to avoid singularity issues in the computation of eq A6, we replace u^{ff}_{LJ2G} by its structurally consistent soft-core form $u^{ff}_{LJ2G-Soft}$, i.e.,

$$U^{ff}_{LJ2G}(z) = \int_0^L 2\pi c(z')\left(\int_{|z-z'|}^{\infty} u^{ff}_{LJ2G-Soft}(r)\, r\, dr\right)dz' \quad (A7)$$

In this work, we solve the integral over z' in eq A7 numerically, and the integral over r is computed by substituting eq 10 for $u^{ff}_{LJ2G-Soft}$ as

$$\int_{|z-z'|}^{\infty} u^{ff}_{LJ2G-Soft}(r)\, r\, dr = \begin{cases} I_{soft}(r)\Big|_{R_{crit}}^{R_{min}} + I_{LJ2G}(r)\Big|_{R_{min}}^{\infty}, & |z-z'| \le R_{crit} \\ I_{soft}(r)\Big|_{|z-z'|}^{R_{min}} + I_{LJ2G}(r)\Big|_{R_{min}}^{\infty}, & R_{crit} < |z-z'| \le R_{min} \\ I_{LJ2G}(r)\Big|_{|z-z'|}^{\infty}, & R_{min} < |z-z'| \end{cases} \quad (A8)$$

dx.doi.org/10.1021/ct200842c | J. Chem. Theory Comput. 2012, 8, 1828−1840

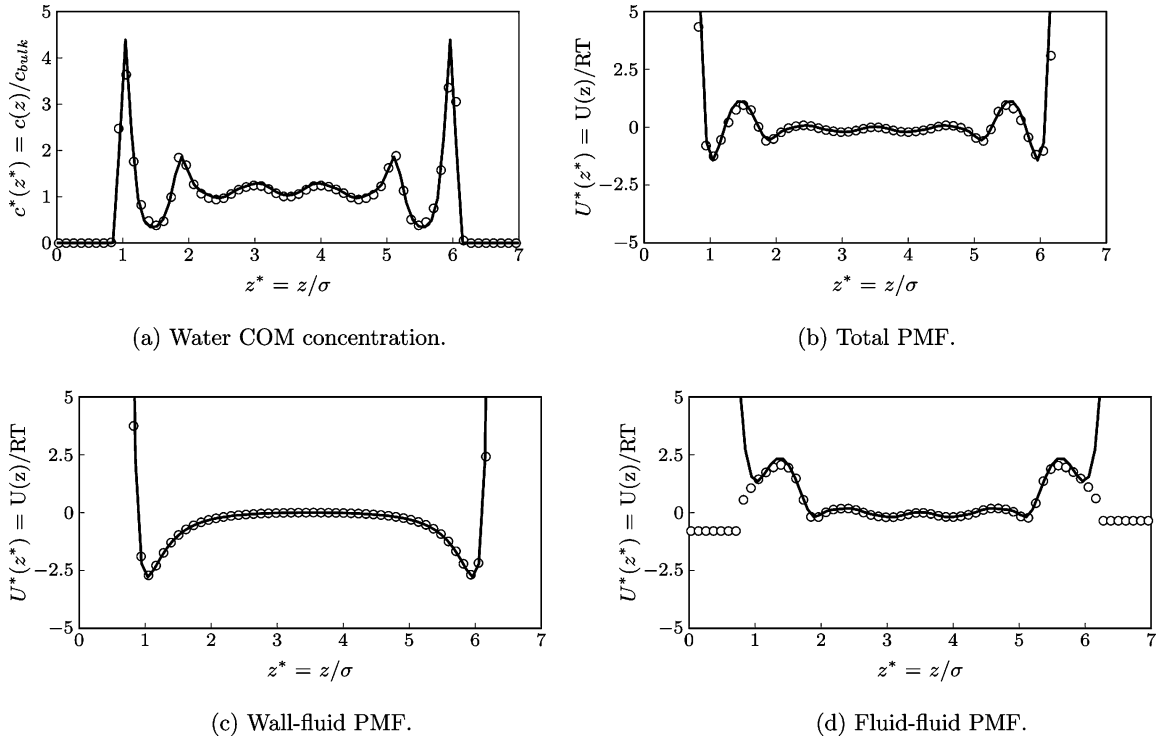

(a) Water COM concentration. (b) Total PMF.

(c) Wall-fluid PMF. (d) Fluid-fluid PMF.

Figure 8. EQT predictions of water COM concentration and potential profiles in the 7σ graphite−water channel. Lines are EQT results, and circles are AA-MD results.

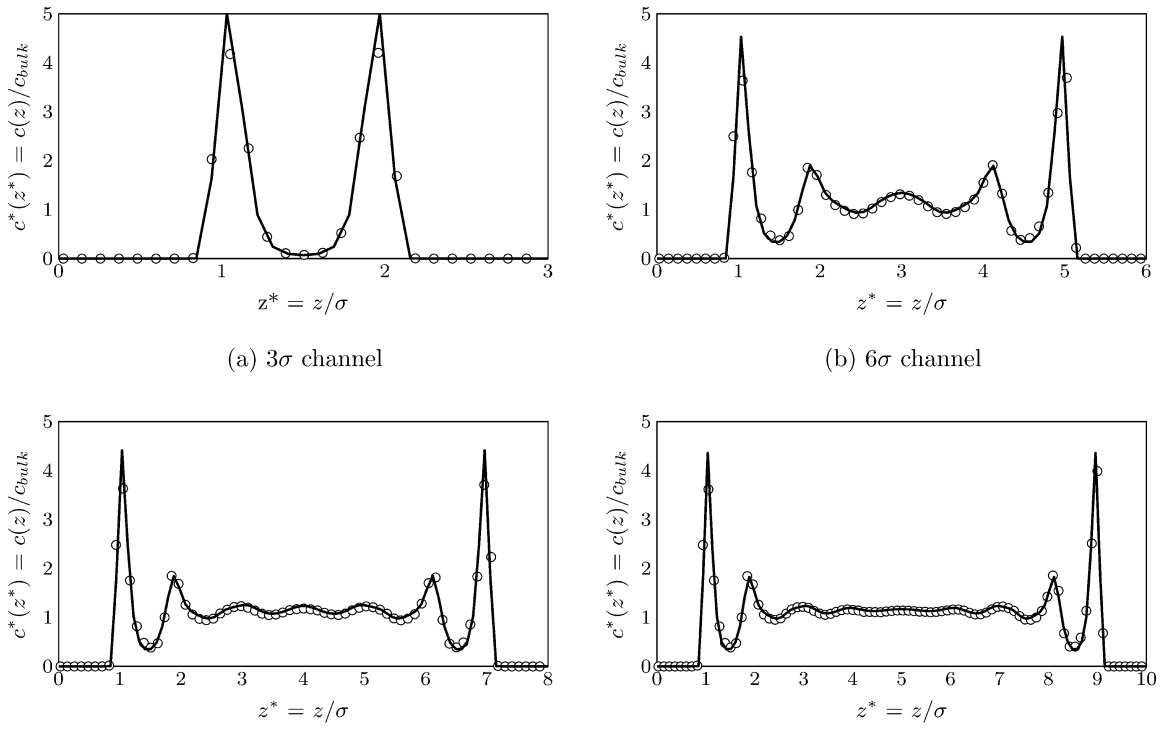

(a) 3σ channel (b) 6σ channel

(c) 8σ channel (d) 10σ channel

Figure 9. Graphite−water channel: EQT predictions of water COM concentration profiles in different channel widths. Lines are EQT results, and circles are AA-MD results.

dx.doi.org/10.1021/ct200842c | J. Chem. Theory Comput. 2012, 8, 1828−1840

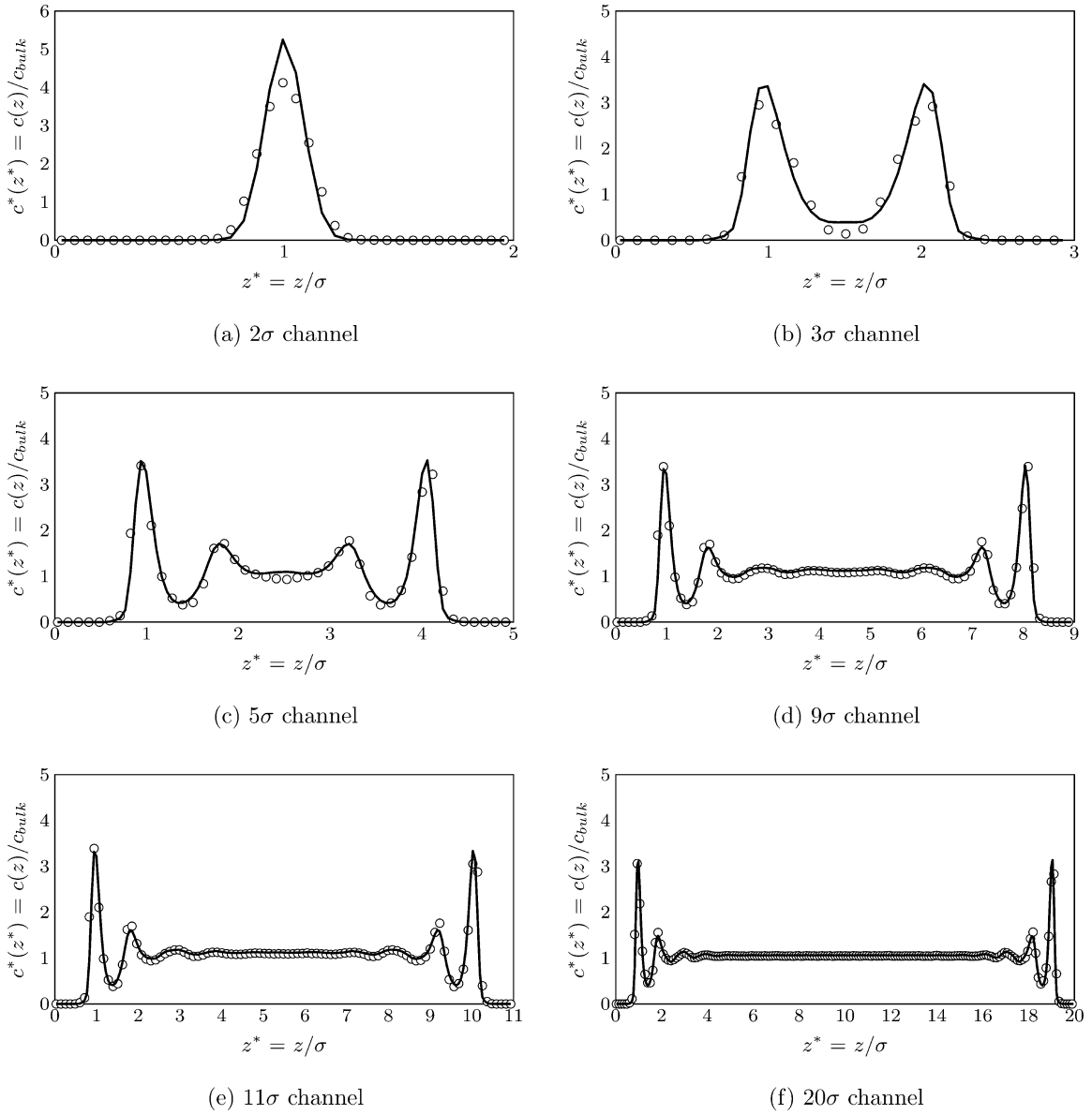

(a) 2σ channel (b) 3σ channel

(c) 5σ channel (d) 9σ channel

(e) 11σ channel (f) 20σ channel

Figure 10. Silicon−water channel: CG-MD predictions of water COM concentration profiles in different channel widths. Lines are CG-MD results, and circles are AA-MD results.

where I_{soft} is given by

$$I_{soft}(r) = \int r(a_0 + a_1(r - R_{min}) + a_2(r - R_{min})^2)dr$$
$$= r^2\left(\frac{a_0}{2} + \frac{a_1}{6}(2r - 3R_{min}) + \frac{a_2}{12}(3r^2 - 8R_{min}r + 6R_{min}^2)\right) \quad \text{(A9)}$$

and I_{LJ2G} is given by

$$I_{LJ2G}(r) = \int\left(4\varepsilon_{ff}\left(\frac{\sigma_{ff}^{12}}{r^{12}} - \frac{\sigma_{ff}^{6}}{r^{6}}\right) + \sum_{i=1}^{2}\lambda_{i,ff}\exp\left(-\left(\frac{r-\mu_{i,ff}}{h_{i,ff}}\right)^2\right)\right)r\,dr$$
$$= 4\varepsilon_{ff}\left(-\frac{\sigma_{ff}^{12}}{10r^{10}} + \frac{\sigma_{ff}^{6}}{4r^{4}}\right)$$
$$-\sum_{i=1}^{2}\frac{\lambda_{i,ff}h_{i,ff}}{2}\left(h_{i,ff}\exp\left(-\left(\frac{r-\mu_{i,ff}}{h_{i,ff}}\right)^2\right) + \sqrt{\pi}\mu_{i,ff}\,\mathrm{erf}\left(\frac{\mu_{i,ff}-r}{h_{i,ff}}\right)\right) \quad \text{(A10)}$$

2. Correction and Wall−Fluid Potential

The correction potential, U_{CGC}^{wf}, can be computed in a similar manner as the fluid−fluid potential, i.e.

$$U_{CGC}^{wf}(z) = \int_{\Gamma_{wall}} 2\pi c_{wall}(z')\left(\int_{|z-z'|}^{\infty} u_{CGC}^{wf}(r)r\,dr\right)dz' \quad \text{(A11)}$$

where Γ_{wall} is defined by the location and the dimensions of the channel walls. Substituting eq 9 for $u_{CGC}^{wf}(r)$ we get

$$\int_{|z-z'|}^{\infty} u_{CGC}^{wf}(r)r\,dr = 4\varepsilon_{CGC}\left(\frac{\sigma_{CGC}^{m}r^{-m+2}}{-m+2} - \frac{\sigma_{CGC}^{n}r^{-n+2}}{-n+2}\right)\Bigg|_{|z-z'|}^{\infty}$$
$$-\sum_{i=1}^{2}\frac{\lambda_{i,CGC}h_{i,CGC}}{2}\left(h_{i,CGC}\exp\left(-\left(\frac{r-\mu_{i,CGC}}{h_{i,CGC}}\right)^2\right)\right.$$
$$\left.+\sqrt{\pi}\mu_{i,CGC}\,\mathrm{erf}\left(\frac{\mu_{i,CGC}-r}{h_{i,CGC}}\right)\right)\Bigg|_{|z-z'|}^{\infty} \quad \text{(A12)}$$

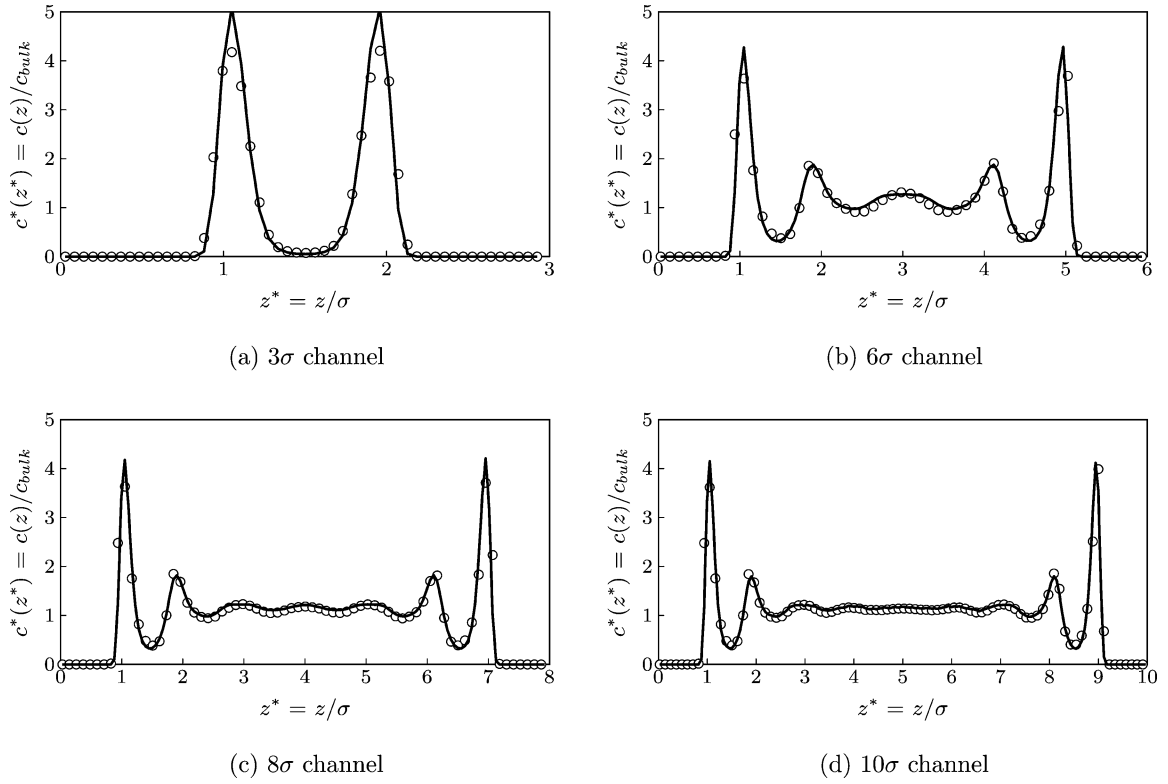

Figure 11. Graphite−water channel: CG-MD predictions of water COM concentration profiles in different channel widths. Lines are CG-MD results, and circles are AA-MD results.

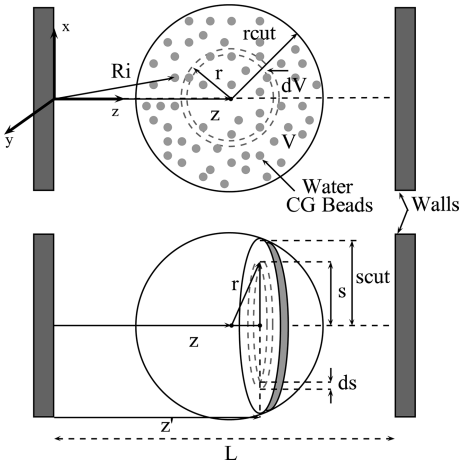

Figure 12. Schematic for EQT potential formulations. Top part shows the atomistic representation, and bottom part shows the continuum representation of a confined fluid.

Similarly, the wall−fluid potential, U_{LJ}^{wf}, can be computed as

$$U_{LJ}^{wf}(z) = \int_{\Gamma_{wall}} 2\pi c_{wall}(z') \left(\int_{|z-z'|}^{\infty} u_{LJ}^{wf}(r) r \, dr \right) dz' \tag{A13}$$

Substituting eq 7 for $u_{LJ}^{wf}(r)$ we get

$$\int_{|z-z'|}^{\infty} u_{LJ}^{wf}(r) r \, dr = 4\varepsilon_{wf} \left(-\frac{\sigma_{wf}^{12}}{10r^{10}} + \frac{\sigma_{wf}^{6}}{4r^{4}} \right) \Bigg|_{|z-z'|}^{\infty} \tag{A14}$$

AUTHOR INFORMATION

Corresponding Author

*E-mail: aluru@illinois.edu.

Notes

The authors declare no competing financial interest.

ACKNOWLEDGMENTS

This work was supported by the NSF under Grants 0328162 (nano-CEMMS, UIUC), 0852657, and 0915718. S.Y.M. wishes to thank Tarun Sanghi for helpful discussions.

REFERENCES

(1) Chaplin, M. F. Structuring and Behaviour of Water in Nanochannels and Confined Spaces. In *Adsorption and Phase Behaviour in Nanochannels and Nanotubes*; Dunne, L. J., Manos, G., Eds.; Springer: Netherlands: Dordrecht, 2010; pp 241−255.

(2) Rasaiah, J. C.; Garde, S.; Hummer, G. *Annu. Rev. Phys. Chem.* **2008**, *59*, 713−740.

(3) Karniadakis, G.; Beskok, A.; Aluru, N. R. *Microflows and Nanofllows: Fundamentals and Simulation*; Springer: New York, 2005.

(4) Qiao, R.; Aluru, N. R. *J. Chem. Phys.* **2003**, *118*, 4692−4701.

(5) Guillot, B. *J. Mol. Liq.* **2002**, *101*, 219−260.

(6) Jorgensen, W. L.; Tirado-Rives, J. *Proc. Natl. Acad. Sci. U.S.A.* **2005**, *102*, 6665−6670.

(7) Attinger, S.; Koumoutsakos, P. *Multiscale Modeling and Simulation*; Springer: New York, 2004.

(8) RuÂhle, V.; Junghans, C.; Lukyanov, A.; Kremer, K.; Andrienko, D. *J. Chem. Theory Comput.* **2009**, *5*, 3211−3223.

(9) Izvekov, S.; Voth, G. A. *J. Chem. Phys.* **2005**, *123*, 134105−134113.

(10) Chaimovich, A.; Shell, M. S. *Phys. Chem. Chem. Phys.* **2009**, *11*, 1901−1915.

(11) Johnson, M. E.; Head-Gordon, T.; Louis, A. A. *J. Chem. Phys.* **2007**, *126*, 144509.

(12) Wang, H.; Junghans, C.; Kremer, K. *Eur. Phys. J. E* **2009**, *28*, 221−229.
(13) Yan, Z.; Buldyrev, S. V.; Giovambattista, N.; Debenedetti, P. G.; Stanley, H. E. *Phys. Rev. E* **2006**, *73*, 051204.
(14) Malani, A.; Ayappa, K. G.; Murad, S. *J. Phys. Chem. B* **2009**, *113*, 13825−13839.
(15) Raghunathan, A. V.; Park, J. H.; Aluru, N. R. *J. Chem. Phys.* **2007**, *127*, 174701.
(16) Sanghi, T.; Aluru, N. R. *J. Chem. Phys.* **2010**, *132*, 044703.
(17) Sanghi, T.; Aluru, N. R. *J. Chem. Phys.* **2012**, *136*, 024102.
(18) Zhou, S. *J. Chem. Phys.* **2009**, *131*, 134702.
(19) Wu, J. *AIChE J.* **2006**, *52*, 1169−1193.
(20) Ravikovitch, P.; Vishnyakov, A.; Neimark, A. *Phys. Rev. E* **2001**, *64*, 011602.
(21) Zhao, S.; Jin, Z.; Wu, J. *J. Phys. Chem. B* **2011**, *115*, 6971−6975.
(22) Kjellander, R.; Greberg, H. *J. Electroanal. Chem.* **1998**, *450*, 233−251.
(23) Das, S. K.; Sharma, M. M.; Schechter, R. S. *J. Phys. Chem.* **1996**, *100*, 7122−7129.
(24) Hess, B.; Kutzner, C.; van der Spoel, D.; Lindahl, E. *J. Chem. Theory Comput.* **2008**, *4*, 435−447.
(25) Berendsen, H. J. C.; Grigera, J. R.; Straatsma, T. P. *J. Phys. Chem.* **1987**, *91*, 6269−6271.
(26) Darden, T.; York, D.; Pedersen, L. *J. Chem. Phys.* **1993**, *98*, 10089−10092.
(27) Nose, S. *J. Chem. Phys.* **1984**, *81*, 511−519.
(28) Rzepiela, A.; Louhivuori, M.; Peter, C.; Marrink, S. *Phys. Chem. Chem. Phys.* **2011**, *13*, 10437−10448.
(29) Louis, A. A. *J. Phys.: Condens. Matter* **2002**, *14*, 9187−9206.
(30) Meyer, H.; Biermann, O.; Faller, R.; Reith, D.; Muller-Plathe, F. *J. Chem. Phys.* **2000**, *113*, 6264−6275.
(31) Reith, D.; Pütz, M.; Müller-Plathe, F. *J. Comput. Chem.* **2003**, *24*, 1624−1636.
(32) Eslami, H.; Karimi-Varzaneh, H. A.; Müller-Plathe, F. *Macromolecules* **2011**, *44*, 3117−3128.
(33) Head-Gordon, T.; Stillinger, F. H. *J. Chem. Phys.* **1993**, *98*, 3313−3327.
(34) Cho, C. H.; Singh, S.; Robinson, G. W. *Faraday Discuss.* **1996**, *103*, 19−27.
(35) Garde, S.; Ashbaugh, H. S. *J. Chem. Phys.* **2001**, *115*, 977−982.
(36) Marti, J.; Nagy, G.; Gordillo, M. C.; Guàrdia, E. *J. Chem. Phys.* **2006**, *124*, 94703.
(37) Head-Gordon, T. *Chem. Phys. Lett.* **1994**, *227*, 215−220.
(38) Rühle, V.; Junghans, C. *Macromol. Theory Simul.* **2011**, *20*, 472−477.